EARTH SURFACE PROCESSES AND LANDFORMS
*Earth Surf. Process. Landforms* **41**, 1421–1436 (2016)

Published online 20 April 2016 in Wiley Online Library
(wileyonlinelibrary.com) DOI: 10.1002/esp.3934

# Characterizing turbulent wind flow around dryland vegetation

**Jerome R. Mayaud,* Giles F.S. Wiggs, and Richard M. Bailey**
Oxford University Centre for the Environment, University of Oxford, Oxford, UK

Received 24 November 2015; Revised 16 February 2016; Accepted 3 March 2016

*Correspondence to: Jerome R. Mayaud, Oxford University Centre for the Environment, University of Oxford, South Parks Road, Oxford OX1 3QY, UK. E-mail: jerome.mayaud@ouce.ox.ac.uk


ESPL
Earth Surface Processes and Landforms

ABSTRACT: Wind flow has been studied in situations where it encounters porous and solid windbreaks, but there has been a lack of research exploring turbulent wind dynamics around and in the lee of real vegetation elements. In dryland contexts, sparse vegetation plays an important role in modulating both the erosivity of the wind and the erodibility of surfaces. Therefore, understanding the interactions between wind and vegetation is key for improving wind erosion modelling in desert landscapes. In this study, turbulent wind flow around three typical dryland vegetation elements (a grass clump, a shrub, and a tree) was examined in Namibia using high-frequency (10 Hz) sonic anemometry. Spatial variations in mean wind velocity, as well as Reynolds stresses and coherent turbulent structures in the flow, were compared and related to the porosities and configurations of the study elements. A shelter parameter, originally proposed by Gandemer (1979, *Journal of Wind Engineering and Industrial Aerodynamic* **4**: 371–389), was derived to describe the combined impact of the different elements on the energy and variability of horizontal wind flow. Wind velocity was reduced by 70% in the immediate lee of the grass and 40% in the lee of the shrub, but velocity recovered exponentially to equilibrium over the same relative distance in both cases (~9 element heights downwind). Quadrant analysis of the high-frequency wind flow data revealed that the grass clump induced a small recirculation zone in its lee, whereas the shrub did not. Also, higher Reynolds shear stress $\left(-\overline{u'w'}\right)$ and higher 'flow positivity magnitude' [ratio of Q1 (outward interaction) and Q4 (sweep) quadrants to Q2 (ejection) and Q3 (inward interaction) quadrants] was generally observed in the wake of the grass. These differences arose because the porosity of the grass clump (53%) was lower than the porosity of the shrub (69%), and thus bleed flow through the shrub was more significant. The bluff-body behaviour of the grass resulted in a more intense and more extensive sheltering effect than the shrub, which implies that overall sediment transport potential is lower in the wake of the grass. The tree displayed a different wake structure to the grass and shrub, owing to the elevation of its crown. A 'bottom gap' effect was observed, whereby wind velocities increased possibly due to streamline compression in the gap between the ground and the underside of the tree crown. Differences in flow momentum between the bottom gap and the low-pressure leeward region of the crown are a probable explanation for the formation of a large recirculation vortex. The bottom gap effect led to decreased sheltering up to three tree heights downwind, but the surface became increasingly protected by the frontal impact of the crown over a further eight tree heights downwind (~30 m). The extraction of momentum from the air by the tree therefore resulted in a far more extensive sheltering effect compared to the grass and shrub. This study represents an important investigation of the impact of different vegetation types on turbulent wind flow, and results can be integrated as parameterizations into spatial sediment transport models that explore landscape-scale change on semi-vegetated desert surfaces. Copyright © 2016 The Authors. Earth Surface Processes and Landforms Published by John Wiley & Sons Ltd.

KEYWORDS: dryland vegetation; turbulent wind flow; sheltering effect; wind erosion; quadrant analysis

## Introduction

### The impact of vegetation on wind flow

The presence of non-erodible roughness elements such as plants significantly complicates wind flow in deserts. By providing drag on the overlying airflow, non-erodible elements affect the velocity profile and thus play a considerable, and sometimes conflicting, role in controlling the erodibility of desert surfaces (Ash and Wasson, 1983; Wasson and Nanninga, 1986; Gillette and Stockton, 1989; Wolfe and Nickling, 1993; Wiggs *et al.*, 1994, 1995; Tegen *et al.*, 2002; MacKinnon *et al.*, 2004; King *et al.*, 2005). Shifts in vegetation structure resulting from grazing, fire and climatic changes are known to have a significant impact on the potential for sediment mobility (Li *et al.*, 2008; Sankey *et al.*, 2012), and therefore have important implications for landscape-scale change in many dryland systems (Thomas *et al.*, 2005; Wang *et al.*, 2009; Stewart *et al.*, 2014).

In dryland contexts, sparse vegetation modulates the erodibility of the surface and the erosivity of the wind through three primary mechanisms (Wolfe and Nickling, 1993). First, vegetation can directly shelter sediment from the wind by

covering a fraction of the surface and providing a lee-side wake (e.g. Al-Awadhi and Willetts, 1999; Leenders *et al.*, 2007). Second, vegetation acts to trap windborne particles, thus reducing flux and providing loci for sediment deposition (e.g. Gillies *et al.*, 2000, 2014; Okin *et al.*, 2006; Davidson-Arnott *et al.*, 2012). Finally, vegetation directly affects wind velocity profiles by acting as a form of roughness, thus simultaneously extracting momentum from surface wind and increasing wind shear velocity above the canopy (e.g. Wasson and Nanninga, 1986; Gillette and Stockton, 1989; Gillies *et al.*, 2002; Crawley and Nickling, 2003; Gillette *et al.*, 2006; Dupont *et al.*, 2014).

Roughness elements shed turbulent eddies in a way that causes the flow in the wake to be separated from the surrounding flow (Wolfe and Nickling, 1993). For smooth, solid objects the interaction with the flow is relatively predictable (van Gardingen and Grace, 1991), but characterizing flow around live plants that are porous, pliable and of diverse geometry, is significantly more complex. Using wind tunnel data, Judd *et al.* (1996) built on the work of Wolfe and Nickling (1993) to classify zones of flow around single porous roughness elements. As wind approaches an obstacle, the air in the layer below the top of the element slows down and diverges upwind, with some air continuing through the porous obstacle to create a region of slower bleed flow in its immediate lee. A low-velocity zone forms in the sheltered area of the obstacle, where wind velocity drastically decreases or even reverses in direction to form a recirculating eddy. Above and downwind of the low-velocity zone, a turbulent mixing zone grows downward from a thin layer at the top of the obstacle, and intersects the ground surface downwind. Eventually the mixing zone merges into an equilibration zone as the airflow recovers to equate to the upwind profile.

The model of Judd *et al.* (1996) has subsequently been supported by wind tunnel data (e.g. Sutton and McKenna-Neuman, 2008; Suter-Burri *et al.*, 2013; Lee *et al.*, 2014; Wu *et al.*, 2015), but few studies have sought to examine the turbulence generated by dryland plants in the field. The exception is Leenders *et al.* (2007), who observed distinct zones of flow acceleration and deceleration around single desert shrubs and a tree in the Sahel. Leenders *et al.* (2007) showed that time-averaged turbulence intensity was higher in low-velocity zones than at other locations, and concluded that the net effect of a shrub is to reduce wind velocity and trap sand particles near the soil surface. The tree was found to reduce wind velocity more effectively than shrubs due to its greater size.

Whilst theoretical calculations (e.g. Raupach, 1992; Okin, 2008) and experimental measurements (e.g. Minvielle *et al.*, 2003; Leenders *et al.*, 2007; Youssef *et al.*, 2012; Gillies *et al.*, 2014; Wu *et al.*, 2015) suggest that protective wakes downwind of vegetation elements extend to approximately 7–10 *h* (where *h* is the height of the element), this can vary significantly depending on plant porosity and pliability. Much of the research on the effects of porosity has been conducted on sand fences and windbreaks, and findings from these are of some relevance to plants (Grant and Nickling, 1998; Leenders *et al.*, 2007). Taylor (1988) found that drag coefficients decreased exponentially as the porosity of a two-dimensional (2D) barrier increased, but Grant and Nickling (1998) demonstrated that a peak in drag coefficient occurred at an intermediate optical porosity (~20%) for three-dimensional (3D) trees. It has been shown that elements with a porosity less than 20% act to enhance wind speed recovery in their lee (Wang and Takle, 1996; Kim and Lee, 2002; Vigiak *et al.*, 2003; Cornelis and Gabriels, 2005), so elements with intermediate porosity strike a compromise between shear stress reduction and the downwind distance for which it is effective (Musick *et al.*, 1996; Lee *et al.*, 2002). However, even porosity values of 50% can cause wake effects to extend to at least 50 *h* downwind of a windbreak (Bradley and Mulhearn, 1983). Some pliable plant stems alter their form to become more streamlined in higher winds, thus extracting momentum less effectively as wind velocities increase (Gillies *et al.*, 2000), and decreasing their sheltering effect (Burri *et al.*, 2011; Walter *et al.*, 2012). Trees affect wind flow and sediment trapping differently to grasses and shrubs, owing to their trunk and crown (Gross, 1987; Leenders *et al.*, 2007; Dupont *et al.*, 2014; Lee *et al.*, 2014), but this has rarely been investigated in the field.

Although windbreak studies are useful for framing research on aeolian dynamics around vegetation elements, the 3D nature of live plants (as opposed to the two-dimensional problem represented by a fence) complicates these interactions (Leenders *et al.*, 2007). In particular, the impact of vegetation on flow turbulence remains a poorly understood phenomenon, especially in field situations where the dynamic complexity of the flow structures cannot be controlled in the same way as in modelled or wind tunnel environments (Clifford and French, 1993). This issue is pertinent given the increasing evidence that turbulence is an important driving force behind sediment entrainment and transport in aeolian environments (Butterfield, 1991, 1993; Sterk *et al.*, 1998; Namikas, 2003; Schönfeldt and von Löwis, 2003; Baas and Sherman, 2005; Leenders *et al.*, 2005; Baddock *et al.*, 2011; Weaver and Wiggs, 2011; Wiggs and Weaver, 2012).

Wind erosion models form a key part of our understanding of sediment transport dynamics on partly vegetated surfaces, and are crucial for assessing the potential vulnerability of dryland regions to soil degradation (Okin *et al.*, 2006; Ravi *et al.*, 2011). However, the current lack of field-based research on turbulence around desert plants hinders the accuracy of wind flow parameterizations in these models. Therefore, the objectives of this study are:

i. to characterize spatial variations of wind velocity and turbulence around three key dryland vegetation elements (a grass, a shrub, and a tree);
ii. to relate any differences in flow properties to the characteristics of the vegetation elements;
iii. to connect observations of turbulent wind patterns, vegetation form and potential zones of enhanced aeolian erosion/deposition in a more formalized way.

The overall aim is to provide empirical data on the impact of vegetation on wind flow, in order to provide appropriate parameterizations of sediment transport potential in large-scale models of dryland landscape evolution. This will help to improve current understanding of how environmental and anthropogenic changes can impact processes occurring on semi-vegetated desert surfaces.

## Methods

### Field sites

The field study was carried out in two locations in Namibia (see Figure 1a). A grass experiment ($Gr_{sonic}1$) and shrub experiment ($Sh_{sonic}1$) were conducted in the southwest Kalahari Desert, ~4 km north of the Auob River (0369913 E, 7180634 N), and a tree experiment ($Tr_{sonic}1$) was conducted on the edge of the Sperrgebiet Reserve in the southern Namib Desert (0619715 E 7045842 N). The Kalahari Desert site was in a farmer's field on raised, flat terrain populated mainly by *Stipagrostis amabilis* grasses, *Rhigozum trichotomum* shrubs and *Acacia erioloba* trees. A wide strip of grazed land meant that the experiments had a fetch of $> 500$ m. The Namib Desert site comprised a large sandy gravel sheet and was populated by patterned

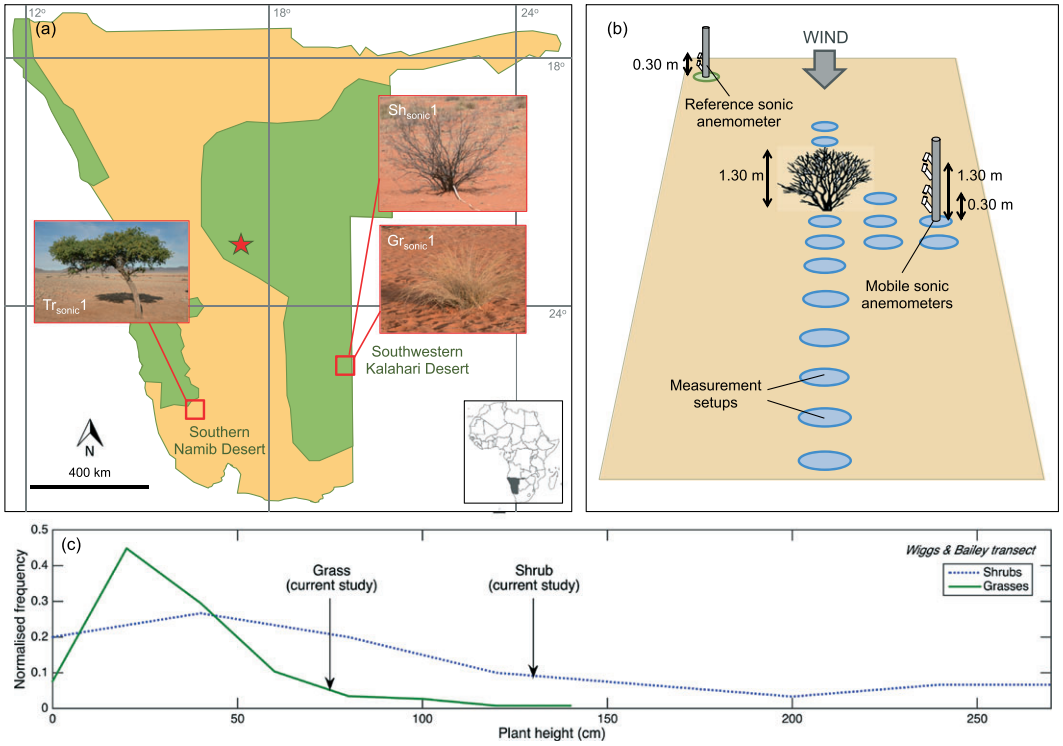


**Figure 1.** (a) Locations of the two field sites in Namibia, and general characteristics of the three study elements. (b) Example of experimental setup for Sh$_{sonic}$1. (c) Frequency distribution of grass and shrub heights along a transect in the southwest Kalahari (Wiggs and Bailey - see Table II for more details). The heights of the grass and shrub in the present study are also indicated. This figure is available in colour online at wileyonlinelibrary.com/journal/espl

shrubby and grassy vegetation, with some sparsely distributed *Acacia erioloba* trees.

Gr$_{sonic}$1 was conducted around a *Stipagrostis amabilis* grass of 0.75 m height, Sh$_{sonic}$1 around a *Rhigozum trichotomum* shrub of 1.30 m height, and Tr$_{sonic}$1 around an *Acacia erioloba* tree of 3.70 m height (see Table I for vegetation characteristics). The three vegetation elements were chosen to be representative of their surrounding populations in terms of height, width and porosity. Table II summarizes plant height and width ranges reported in previous field studies, as well as average plant characteristics along vegetation transects conducted at each field site (A) and at five other sites located < 150 km away from the Kalahari site (B). The frequency distribution of grass and shrub heights along the latter transects are shown in Figure 1c. The three vegetation elements in this study fall within the majority of reported height/width ranges, and the grass and shrub elements in this study had a standard ($Z$) score of 1.32 and 0.44, respectively, relative to the distributions in Figure 1c. The study elements are therefore considered to be generally representative of their surrounding environments.

The optical porosity of the study elements was determined using a digital photogrammetry method adapted from Kenney (1987). Digital photographs of part of the canopy were taken at approximately 0.40 m from shrubs and grasses, and 3.0 m from tree canopies, using a Nikon D3100 DSLR camera with a resolution of 14.2 Megapixels, from the principal wind direction (thus accounting for the plant structures that the wind interacts with directly). The photographs were enlarged to fill the image dimensions, converted to greyscale images, and the perimeter of the plant was defined using a polygon that was inputted into the code manually. A variety of threshold values for black (plant branches) and white (open area) pixels were calculated, and the best fit to actual element shape was visually determined (cf. Gillies *et al.*, 2000; Leenders *et al.*, 2007). The percentage of white pixels, averaged across all directions, was taken as the mean optical porosity of the element canopy.

## Experimental setup

Three 3D sonic anemometers (Campbell CSAT-3) were deployed around each study element to collect wind velocity data ($u$, horizontal; $v$, spanwise; and $w$, vertical) at a sampling frequency of 10 Hz. A mobile anemometer array was erected with two sonic anemometers fixed onto a mobile steel mast: one at 0.30 m height, which is low enough to capture turbulence potentially responsible for surface entrainment whilst minimizing the interference of saltating sand with the sonic measurement path (Weaver and Wiggs, 2011), and another at the height of the vegetation element (restricted to 1.50 m for the tree experiment due to mast height limitations). The third sonic anemometer was mounted at 0.30 m height and placed 20 $h$ upwind and 15 $h$ to the side of the experimental plot in a non-distorted environment (i.e. with a significant fetch over a flat, bare surface). This provided reference wind data against which mobile anemometry data could be normalized. Practicality constraints meant that data collected at the height of each vegetation element was normalized against reference data measured at 0.30 m height (the normalization of wind velocities at multiple heights using a single reference height is common practice; e.g. Wiggs and Weaver, 2012). The anemometers were all aligned parallel with the prevailing wind direction and level in the horizontal plane. The experimental setup of Gr$_{sonic}$1 is shown in Figure 1b as an illustrative example.

The mobile mast was moved within a grid formation upwind, downwind and to the sides of each element, oriented in the direction of the wind. Each grid was divided into a number of measurement setups, during which both mobile anemometers

**Table I.** Descriptive experimental statistics for the three sonic anemometry experiments around single vegetation elements, as measured at the reference anemometer at 0.30 m height

| Experiment | Date | Species | Height (m) | Width (m) | Optical porosity (%) | $u$ (m s$^{-1}$) during experiment | | | | $u$ (m s$^{-1}$) during entire month | | | |
|---|---|---|---|---|---|---|---|---|---|---|---|---|---|
| | | | | | | Minimum | Maximum | Mean | Standard deviation | Minimum | Maximum | Mean | Standard deviation |
| $Gr_{sonic}1$ | 27 September 2014 | *Stipagrostis amabilis* (Grass) | 0.75 | 1.30 | 53 | 1.72 | 4.83 | 3.02 | 0.72 | 0.00 | 8.81 | 1.32 | 1.21 |
| $Sh_{sonic}1$ | 30 September 2014 | *Rhigozum trichotomum* (Shrub) | 1.30 | 1.80 | 69 | 0.89 | 4.22 | 2.64 | 0.73 | | | | |
| $Tr_{sonic}1$ | 23 September 2014 | *Acacia erioloba* (Tree) | 3.70 (trunk: 2.30; crown: 1.40) | 5.20 | 6 | 1.22 | 4.33 | 2.97 | 0.62 | 0.00 | 8.77 | 2.45 | 1.73 |

Note: Width is given as the length of the element axis perpendicular to the axis of the experimental plot. Tree porosity refers to the porosity of the crown. Also shown are monthly wind velocity data measured at 0.30 m height at the same field sites (17 August 2014–15 September 2014 in the southwest Kalahari; 16 September 2014–5 October 2014 in the southern Namib).

simultaneously recorded wind velocity. To ensure sufficient data were acquired for subsequent analysis, each setup was run for a minimum of 20 minutes. The alignment of the experimental plot relative to the wind was altered after every instrumental setup to reflect any minor wind directional changes, and any misaligned data were removed in subsequent analysis (see Data analysis section). Throughout this study, annotation for measurement locations is given as $h_d$ (downwind distance) and $h_L$ (lateral distance) in terms of the height of the element. Wind flow was measured from $-2h_d$ (i.e. upwind) to 11–18$h_d$ depending on the element, and up to $2h_L$. Lateral wind flow was only measured on one side of each element, as wind dynamics were considered to be effectively symmetrical about the centreline of the wake (Leenders *et al.*, 2007).

## Data analysis

The three experiments were carried out on separate windy days in September 2014 (Table I). Mean approach (i.e. reference) wind velocities during the experiments ranged from 2.64 m s$^{-1}$ to 3.02 m s$^{-1}$, which was representative of the average conditions measured at the same field sites over a period of approximately one month. In order to ensure that the airflow detected at each measurement location had interacted as much as possible with the study element, the datasets were filtered to exclude oncoming wind directions $> 5°$ from the centreline of the experimental plot. Previous work on turbulent wind flows has shown that sampling periods for velocity measurements must be long enough to capture the full range of turbulent eddies, and thus be representative of the processes occurring in the boundary layer. Van Boxel *et al.* (2004) recommend that for an average wind velocity of 2.50 m s$^{-1}$ and observation heights up to 1.50 m, a convenient sampling period is on the order of four to seven minutes. The mean number of minutes per measurement setup (after being filtered using the 5° threshold) ranged from 6.6 minutes to 8.6 minutes, thus conforming to van Boxel *et al.*'s (2004) recommendation. Across all measurement setups, the total number of data points at each measurement height was 56 160 ($Gr_{sonic}1$), 63 900 ($Sh_{sonic}1$) and 46 200 ($Tr_{sonic}1$). Unless otherwise stated, all wind flow parameters were normalized against the mean wind velocity ($\overline{U}$) recorded by the upwind reference anemometer at 0.30 m height. Normalization is indicated using the 'norm' subscript for each parameter.

The sonic anemometer data from all three experiments were post-processed to correct for misalignment errors. The streamwise frame of reference was rotated in accordance with the local streamline angle using yaw rotation (cf. Frank and Kocurek, 1996; van Boxel *et al.*, 2004; Walker, 2005; Weaver and Wiggs, 2011; Chapman *et al.*, 2012). Roll and pitch rotation were omitted from the correction procedure because the streamlines were considered to be horizontal over the desert surface. Subsequent to yaw rotation correction the average spanwise velocity was zero $\left(\overline{V} = 0\right)$, and so no further analysis of this component was undertaken. The remaining velocity data were decomposed into their average $\left(\overline{U}, \overline{V} \text{ and } \overline{W}\right)$ and fluctuating ($u'$, $v'$ and $w'$) components, from which the horizontal $\left(\overline{u'^2}\right)$ and vertical $\left(\overline{w'^2}\right)$ components of Reynolds stress were derived. The Reynolds shear stress $\left(-\overline{u'w'}\right)$ was calculated using the time-averaged covariance of the instantaneous horizontal and vertical turbulent components. The local, near-surface streamline angle ($\theta$) was determined as:

**Table II.** Average plant characteristics for grasses, shrubs and trees in relevant dryland regions, as reported in previous studies and unpublished data from authors

| Study | Location | Plant type | Height (m) | Width (m) | Porosity (%) |
|---|---|---|---|---|---|
| Wiggs *et al.* (1994) | Southwest Kalahari | Grass | 0.8–1.0 | — | — |
| Wiggs *et al.* (1995) | Southwest Kalahari | Grass/shrub | 0.1–0.3 | — | — |
| Wiggs *et al.* (1996a) | Southwest Kalahari | Grass/shrub | 0.3–0.6 | — | — |
| van Rooyen *et al.* (2001) | Southwest Kalahari | Grass | 0.2–2.0 | — | — |
| | | Shrub | 0.5–2.0 | — | — |
| | | Tree | 2.0–6.0 | — | — |
| Thomas and Leason (2005) | Southwest Kalahari | Grass | 0.2–0.3 | — | — |
| Vegetation transects A (current study) | Southwest Kalahari | Grass | 0.1–1.1 | 0.1–1.9 | 31–43 |
| | | Shrub | 0.3–1.7 | 0.5–3.2 | 38–71 |
| | Southern Namib | Shrub | 0.4–1.6 | 0.3–2.1 | 63–69 |
| | | Tree | 3.0–5.5 | 4.0–7.5 | 4–10 |
| Vegetation transects B (Wiggs and Bailey, unpublished) | Southwest Kalahari | Grass | 0.05–1.5 | 0.05–1.3 | — |
| | | Shrub | 0.05–2.9 | 0.1–3.4 | — |
| | | Tree | 1.4–5.1 | 1.1–6.0 | — |

Note: The vegetation transects conducted for this study (A) consisted of eight individual transects of 25 m length and 1 m width at both sites; along each transect, the height, width and porosity of each plant was recorded. The vegetation transects of Wiggs and Bailey (B) were conducted in September 2010 at five separate sites in the southwest Kalahari, each located < 150 km from the current study site.

$$\theta = \arctan\left(\frac{\overline{W}}{\overline{U}}\right) \quad (1)$$

From these parameters, the incidence of coherent structures in the flow around the grass, shrub and tree elements was established using conditional-sampling quadrant analysis (Lu and Willmarth, 1973). This technique defines four discrete categories of momentum exchange based on the relative signs of $u'$ and $w'$. Ejections (Q2 events; $u' < 0$, $w' > 0$) and sweeps (Q4; $u' > 0$, $w' < 0$) contribute positively to the production of Reynolds stress, while outward interactions (Q1; $u' > 0$, $w' > 0$) and inward interactions (Q3; $u' < 0$, $w' < 0$) contribute negatively to Reynolds stress (Smith, 1996). In order to isolate significant bursts of turbulent stress from weaker background variability (Lapointe, 1992; Clifford and French, 1993), stress events of low magnitude were removed from quadrant analysis using a threshold criterion ($H$). Following previous studies (Bauer *et al.*, 1998; Sterk *et al.*, 1998; Leenders *et al.*, 2005; Weaver, 2008; Wiggs and Weaver, 2012), the size of $H$ was chosen to be equivalent to one standard deviation ($\sigma$) of the Reynolds shear stress $\left(-\overline{u'w'}\right)$, such that a flow structure was only classified if $-u'w' > \pm H\left(-\overline{u'w'}\right)$.

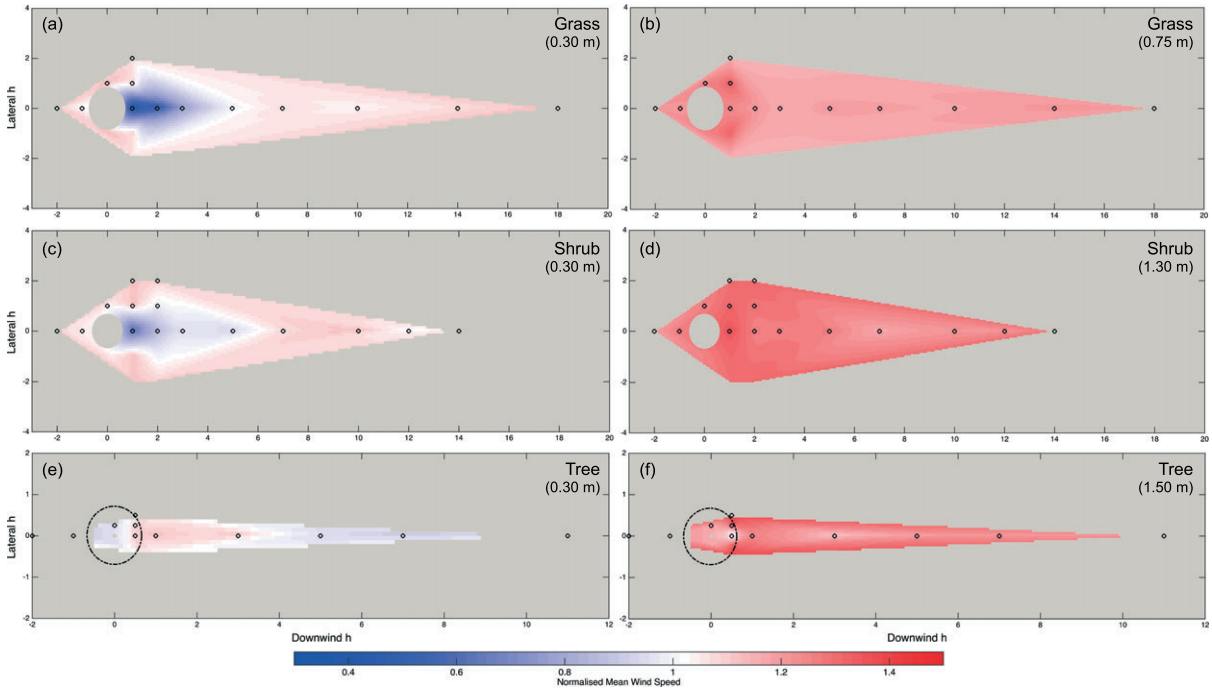


**Figure 2.** Spatial patterns of normalized mean wind velocity ($\Phi$) at 0.30 m and element height (1.50 m for tree) for: (a), (b) a grass clump; (c), (d) a shrub; (e), (f) a tree. Data were interpolated using a triangulation-based natural neighbour algorithm, with a grid spacing of 0.1 m. Location of grass and shrub elements are shown by white ellipses, and tree crown extent is shown as a dotted ellipse. Black circles represent anemometer locations. Downwind $h$ for trees is calculated using total tree height (i.e. trunk + crown). Lateral wind velocity data are mirrored across the centrelines of the element wakes. This figure is available in colour online at wileyonlinelibrary.com/journal/espl

## Results and Discussion

### Mean wind velocity around single vegetation elements

Figure 2 displays the spatial patterns of mean normalized wind velocity ($\Phi$) around the three study elements. Normalized wind velocities at each measurement location were interpolated using a triangulation-based natural neighbour algorithm, with a grid spacing of 0.1 m. This resolution was chosen because the measurement locations around the elements were determined at a scale of 0.1 to 1.0 m. The algorithm was chosen because it produced robust spatial features that were present using several other commonly used interpolation algorithms. Since wind velocity was quantified only on one side of each element in the field, the measured velocities were plotted symmetrically over the centreline of the elements in order to provide better visualization of recovery patterns.

The contour plots at 0.30 m height show clear regions of reduced wind velocity compared to upwind values ($\Phi < 1.0$) in the wakes of the grass (Figure 2a) and the shrub (Figure 2c). These correspond with low-velocity zones previously identified in the lee of windbreaks and other flow obstructions (Judd *et al.*, 1996; Musick *et al.*, 1996; Lee *et al.*, 2002). Wind slowdown was more intense in the lee of the grass compared to the shrub. There was a reduction in wind velocity directly upwind and a slight speedup to the sides of the two elements, although these were minor compared to the slowdown observed along the centreline of the wake.

At the height of the grass and shrub elements, normalized wind velocity was higher in comparison to the surface, because the reference anemometer was placed lower than the mobile anemometer (0.30 m and element height, respectively). In the grass case (Figure 2b), there was some disturbance to the flow up to $2h_d$, with flow accelerating by 6–8% above the grass clump, but recovery to upwind values was almost immediate. In contrast, the wind was more significantly impacted in the case of the shrub (Figure 2d), with flow accelerating by 8–10% above and to the side of the element, and normalized wind velocity remaining high until $5h_d$. These changes are comparable to the wind tunnel results of Wu *et al.* (2015), who found that certain shrub species induce above-canopy flow acceleration of up to 13%. The comparatively limited impact of the grass on mean wind velocity at the element height is likely due to the pliable nature of the grass stems, which alter their form to become more streamlined as wind velocities increase and thus extract momentum less effectively at height (Gillies *et al.*, 2000). Since the shrub was 0.55 m taller than the grass element, wind velocity at shrub height is likely to be higher in absolute terms than at grass height. Given that both datasets were normalized to reference wind flow measured at 0.30 m height, it should be expected that $\Phi$ values are greater at shrub height than at grass height.

The tree, on account of its elevated crown, caused visibly different wind velocity changes when compared with the grass and shrub. At 0.30 m height (Figure 2e), normalized wind velocity decreased upwind and up to $0.5h_d$ of the tree trunk, and was above unity from the downwind edge of the crown until ~$4h_d$. This sub-crown wind speedup has previously been termed the 'bottom gap' effect (Ruck and Schmitt, 1986). The effect arises because wind flowing near the top half of the tree moves over the tree crown (Gross, 1987; Lee *et al.*, 2014), whereas in the lower region of the tree, a dominant downdraft speeds up the wind due to streamline compression in the gap between the ground and the underside of the crown (Kim and Lee, 2002; Dupont *et al.*, 2014). At 1.50 m height (Figure 2f) two zones of relative wind slowdown were observed: one directly beneath the crown, and one between $2h_d$ and $5h_d$. The sonic anemometer at this height was measuring wind flow just 0.80 m below the underside of the crown, so the observed slowdown likely resulted from the frontal impact of the crown being increasingly felt downwind. A localized speedup of wind around the sides of the tree trunk due to lateral streamline compression, as reported in previous studies (e.g. Gross, 1987; Leenders *et al.*, 2007), was not observed in our wind data. This was probably because the closest anemometer to the trunk was too far away (0.90 m) to capture this aerodynamic effect. However, there was some evidence of sediment deflation in the immediate vicinity of the trunk (~0.20 m deflation, extending for ~0.40 m downwind), and this could probably be linked to local wind acceleration.

Figure 3 displays the recovery of normalized mean wind velocity ($\Phi$) at 0.30 m height along the centreline of the three element wakes. The grass and shrub data were fitted using a saturating exponential function, as the recovery of wind flow downwind of an obstruction can generally be described as an exponential curve (Bradley and Mulhearn, 1983). The wind data around the tree was fitted using a logistic function, as this was visually and statistically determined to fit the data most appropriately. The derived functions showed very good fits with the observed values, with high $R^2$ and low sum of square error (SSE) and root-mean-square error (RMSE) values (see table in Figure 3). Also presented are recovery rates published in other studies, assuming an obstacle porosity of 53% (same as the grass element in this study): (i) Hagen's (1996) friction velocity reduction factor behind a windbreak; (ii) Leenders *et al.*'s (2011) adaptation of Hagen's (1996) function for a single shrub; (iii) Okin's (2008; corrected in Li *et al.*, 2013) parameterization of reduced shear stress downwind of a plant, fitted to Bradley and Mulhearn's (1983) empirical data downwind of a wind fence. Although the functions of Hagen (1996) and Okin (2008) were developed to describe friction velocity/shear stress, these parameters are linearly related to wind velocity such that recovery rates should be comparable (Leenders *et al.*, 2011).

With reference to Figure 3, it is clear that wind velocity recovered to equilibrium flow at approximately the same distance (~$9h_d$) downwind of the grass and the shrub, which is comparable to recovery lengths for solitary elements identified in other similar studies (Leenders *et al.*, 2007; Gillies *et al.*, 2014; Wu *et al.*, 2015). However, the overall rate of recovery (i.e. gradient of the best fit line) was higher in the case of the grass, because initial wind slowdown at $1h_d$ of the grass (70% reduction) was larger than that of the shrub (40% reduction). This suggests that the grass acted as more of a bluff body, with the lower porosity of the grass (53%) compared to the shrub (69%) resulting in a higher drag coefficient and thus greater momentum loss in the lee. These data support previous findings (Skidmore and Hagen, 1970; Perera, 1981) that lower-porosity elements induce more intense wind slowdown in their lee but allow flow to recover to upstream conditions sooner than more porous elements. Starting from $\Phi = 1.2$ (due to wind speedup caused by the 'bottom gap' effect as previously discussed), wind velocity downwind of the tree experienced an increasing decline until ~$4h_d$, followed by a reduced rate of slowdown until equilibration at ~$7h_d$ (26 m). The initially rapid rate of slowdown can be attributed to the frontal impact of the elevated crown being increasingly felt at the surface. The height of the trunk likely dictates the downwind distance at which the effect of the crown is first detected at the surface, and the height of the crown determines the distance over which the wind velocity recovers back to $\Phi = 1.0$.

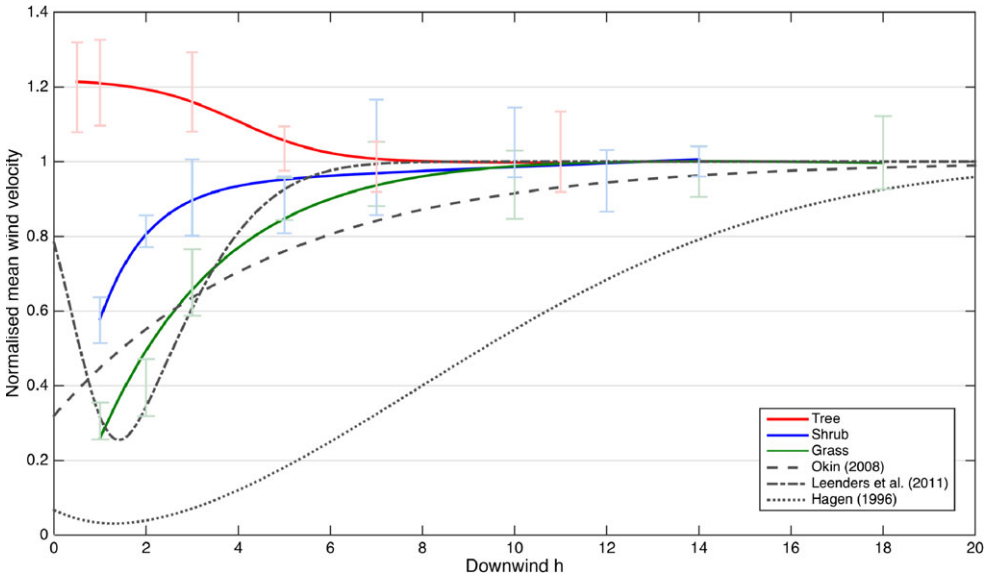


| Element | Function | Coefficient values | | | | Goodness of fit | | |
|---|---|---|---|---|---|---|---|---|
| | | a | b | c | d | SSE | $R^2$ | RMSE |
| Grass | $ae^{-bx} + c$ | -1.099 | 0.3849 | 1.106 | - | 0.0202 | 0.964 | 0.0636 |
| Shrub | $ae^{-bx} + c$ | -0.8837 | 0.7162 | 1.054 | - | 0.0158 | 0.914 | 0.0561 |
| Tree | $a + (b\text{-}c)/(1 + e^{x-d}))$ | 0.9176 | 7.814 | 7.608 | 3.967 | 0.0023 | 0.948 | 0.0339 |

**Figure 3.** Best fit regression lines for normalized mean wind velocity ($\Phi$) downwind of the study elements at 0.30 m height. Error bars represent the standard deviation of the mean. Also shown are the models of Okin (2008) and Leenders *et al.* (2011) for porous shrubs, and of Hagen (1996) for a porous windbreak. A porosity of 53% is assumed for the Leenders *et al.* (2011) and Hagen (1996) models. Table displays function form, coefficients and goodness-of-fit statistics for the general fitting models. This figure is available in colour online at wileyonlinelibrary.com/journal/espl

The recovery curves derived from the grass and shrub data in this study compared relatively well to the Leenders *et al.* (2011) formulation for wind velocity recovery downwind of a shrub, although wind speedup occurs more rapidly and equilibrium reached sooner in the Leenders *et al.* (2011) model. This difference can be ascribed to the lower optical porosity (18%) of the test shrub in the Leenders study, which, as discussed earlier, is thought to induce a faster recovery of wind velocity over a given distance. The decrease in normalized wind velocity between $0h_d$ and $1h_d$ simulated by the Leenders *et al.* (2011) model could not be verified, as wind was not measured closer than $1h_d$ in this study, but the location of minimum wind velocity is likely also located in this zone in the case of our grass and shrub. The recovery rates simulated by the models of Hagen (1996) and Okin (2008) were much slower than the rates observed in this study, with normalized wind velocity reaching equilibrium at $21h_d$ and $18h_d$, respectively. This implies that two-dimensional wind fences may not be suitable analogues for three-dimensional, partially bluff forms such as grasses and shrubs, as concluded by Gillies *et al.* (2014) for nebkha dunes and Lee *et al.* (2014) for single trees. The recovery curve of the tree in this study was not well simulated by any of the presented models, because none of them allows $\Phi$ to rise above 1.0 in an element's wake, such that wind speedup associated with the 'bottom gap' effect is not accounted for.

## Turbulence around single vegetation elements

While mean wind velocity data provide some information about vegetative impacts on flow, turbulent variations must also be considered when characterizing different zones of flow around individual elements, because there is increasing evidence that turbulence is an important driving force behind aeolian sediment entrainment and transport in complex flows (Butterfield, 1991; Sterk *et al.*, 1998; Schönfeldt and von Löwis, 2003; Leenders *et al.*, 2005, 2007; Wiggs and Weaver, 2012). Reynolds stresses provide a direct representation of turbulent fluctuations by accounting for instantaneous deviations from the mean flow, and these stresses have to some extent been related to sediment transport dynamics at the dune scale (Baddock *et al.*, 2011; Weaver and Wiggs, 2011; Chapman *et al.*, 2012). Investigating the spatial variability of turbulent stresses around plants is therefore useful for identifying specific zones of potential erosion/deposition on partially vegetated surfaces.

Figure 4 shows how the distribution of horizontal wind velocity (measured at 10 Hz) at 0.30 m height around the study elements changed relative to the approach flow. Student's *t*-test results suggest that the mean wind velocities measured downwind and to the sides of the elements were in most cases significantly different ($p < 0.001$) to the approach flow, although the clearest differences were observed in the immediate lee of the grass and shrub. Chi-squared tests comparing the entire wind velocity distributions at each measurement location with the approach flow reveal that significant differences (at the 95% level) only occurred in the lee of the grass and shrub up to $2h_d$. In this region, the centres of the distributions were shifted to lower wind velocities, resulting in skewness values that were up to 63% higher (i.e. more positive) than the skewness of the approach flow. Increased positive skewness is caused by infrequent, intermittent events of accelerated fluid with respect to the ambient flow, and is an indicator of elevated turbulence within the flow (Sterk, 2000).

Figure 5 displays the spatial variations of normalized horizontal normal Reynolds stress $\left(\overline{u'^2}_{norm}\right)$ around the study elements. Vertical velocity variations were roughly an order of

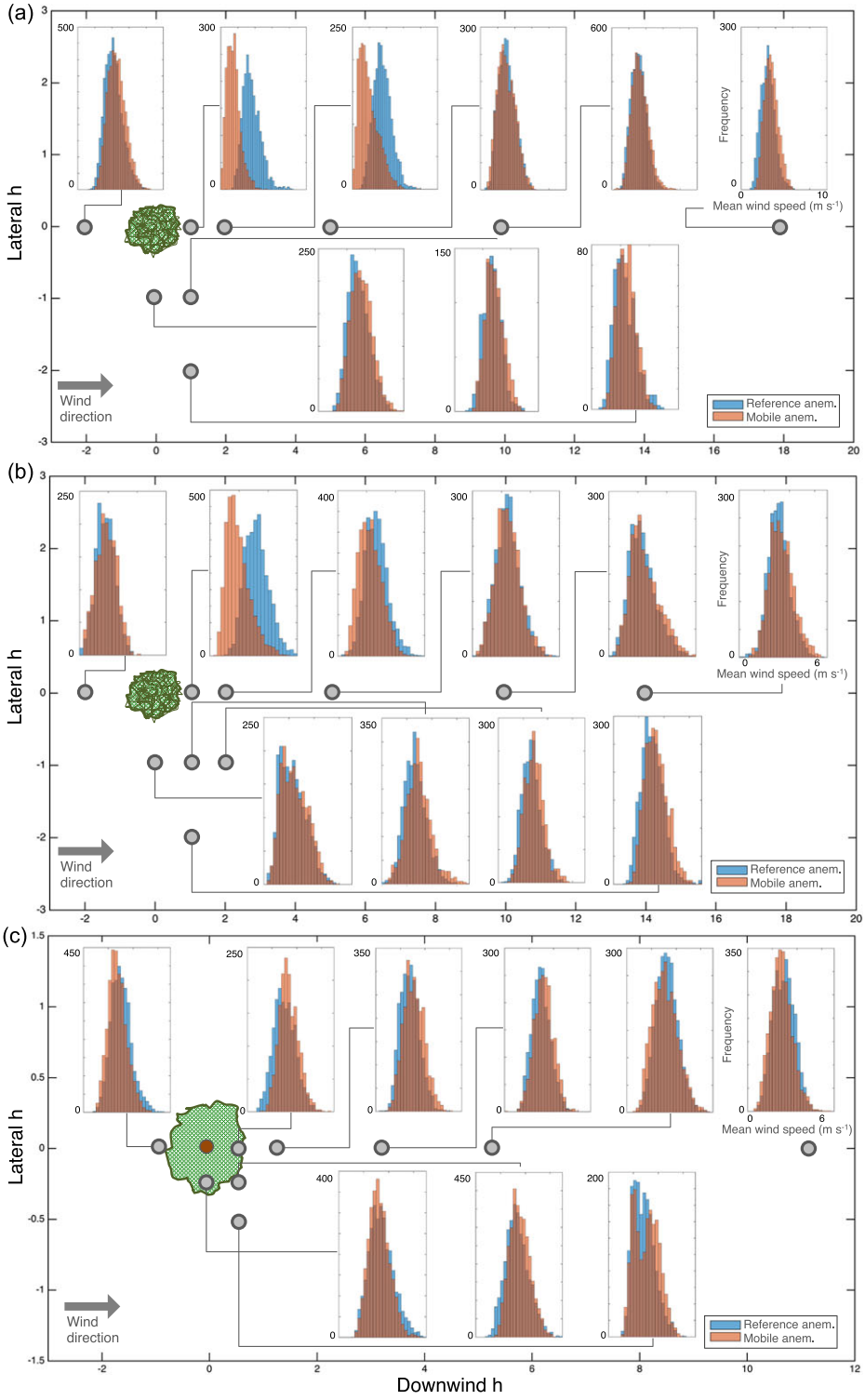


**Figure 4.** Horizontal wind velocity distributions for instantaneous 10 Hz sonic anemometry data at 0.30 m height, at different locations around: (a) a grass; (b) a shrub; (c) a tree. Anemometer locations are shown as grey circles. Vegetation element location is shown as green ellipse. Histograms for reference and mobile sonic anemometers are shown. This figure is available in colour online at wileyonlinelibrary.com/journal/espl

magnitude smaller than the horizontal components of flow in this study (cf. Sterk *et al.*, 1998; van Boxel *et al.*, 2004; Leenders *et al.*, 2005; Weaver and Wiggs, 2011), so vertical normal Reynolds stress $\left(\overline{w'^2}\right)$ data are not presented. Downwind of the grass (Figures 5a and 5b), $\overline{u'^2}_{norm}$ peaked at $3h_d$ at element height and at $7h_d$ at the surface. In contrast, $\overline{u'^2}_{norm}$ was low in the lee of the shrub at both heights and peaked at $12h_d$ (Figures 5c and 5d), five element heights further than the grass. Zones of elevated $\overline{u'^2}_{norm}$ occurred to the side of the shrub but not to the side of the grass. The observed regions of elevated stress probably result from counter-rotating vortices induced by the elements, which can act to increase sediment entrainment potential (Sutton and McKenna-Neuman, 2008; Burri *et al.*, 2011). In the case of the tree (Figures 5e and 5f), $\overline{u'^2}_{norm}$ was relatively low beneath the crown at both heights, although a slight increase was observed to the sides of the crown at 1.50 m height, which could also result from small vortices induced by the underside of the canopy.

The spatial variations of normalized Reynolds shear stress $\left(-\overline{u'w'}_{norm}\right)$ around the three elements are shown in Figure 6. The grass clump induced an area of high $-\overline{u'w'}_{norm}$ in its lee

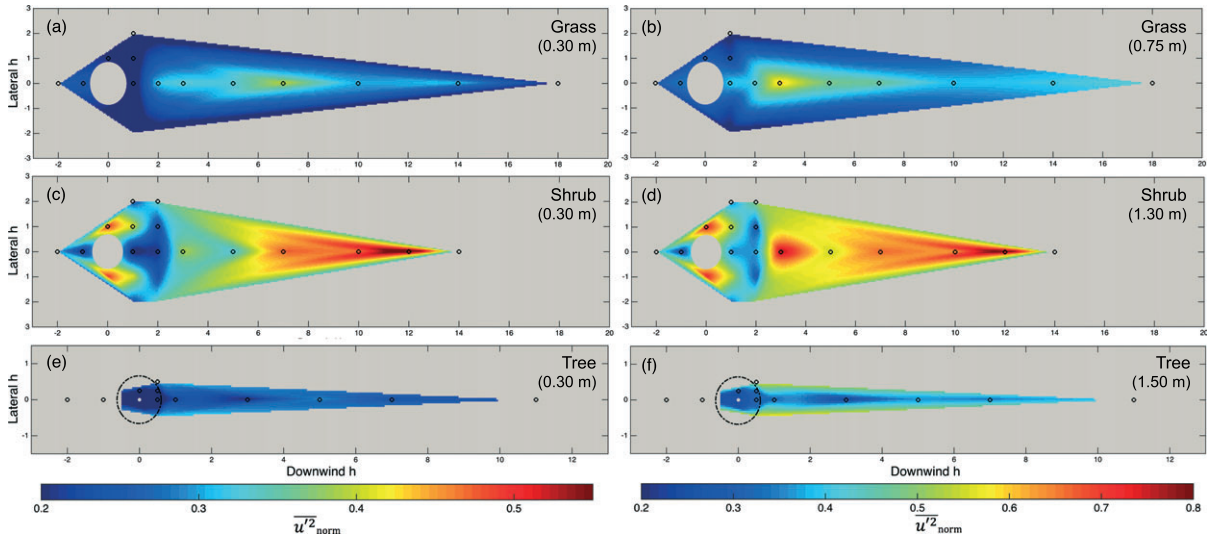


**Figure 5.** Horizontal spatial patterns of average normalized horizontal normal Reynolds stress $\left(\overline{u'^2}_{norm}\right)$ at 0.30 m and element height (1.50 m for tree): (a), (b) a grass; (c), (d) a shrub; (e), (f) a tree. Data were normalized to $\overline{U}$ of an upwind reference anemometer at 0.30 m height, and interpolated using a triangulation-based natural neighbour algorithm, with a grid spacing of 0.1 m. Locations of grass and shrub elements are shown by white ellipses. Tree crown is shown as a dotted ellipse. Black circles represent anemometer locations. Downwind $h$ for the tree is calculated using total tree height (trunk + crown). Lateral turbulence data are mirrored across the centreline of each element wake. This figure is available in colour online at wileyonlinelibrary.com/journal/espl

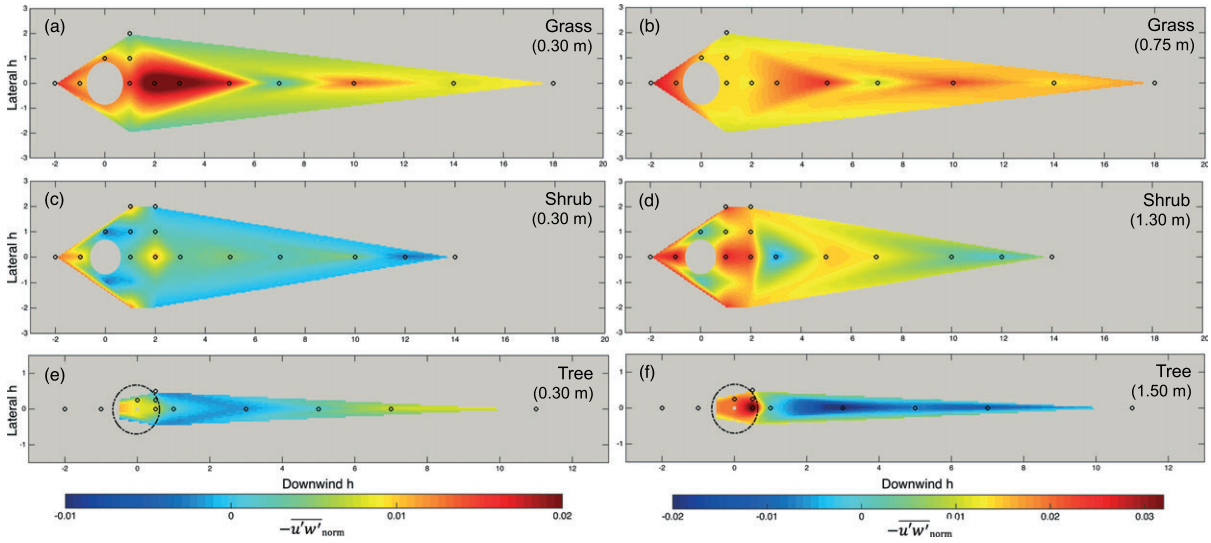


**Figure 6.** Horizontal spatial patterns of average normalized Reynolds shear stress $\left(-\overline{u'w'}_{norm}\right)$ at 0.30 m and element height (1.50 m for tree) for: (a), (b) a grass; (c), (d) a shrub; (e), (f) a tree. Data were normalized to $\overline{U}$ of an upwind reference anemometer at 0.30 m height, and interpolated using a triangulation-based natural neighbour algorithm, with a grid spacing of 0.1 m. Locations of grass and shrub elements are shown by white ellipses. Tree crown is shown as a dotted ellipse. Black circles represent anemometer locations. Downwind $h$ for trees is calculated using total tree height (trunk + crown). This figure is available in colour online at wileyonlinelibrary.com/journal/espl

that was much wider than around the shrub (Figures 6c and 6d), and Reynolds shear stress was generally much lower around the shrub compared to the grass. Results presented in Figures 5 and 6 suggest that by allowing a larger proportion of wind flow to bleed through its canopy, the shrub induced less intense turbulence in its immediate lee than the grass. However, the more significant bleed flow acted to disrupt the airflow further downwind (particularly evident for the $\overline{u'^2}_{norm}$ parameter). Peaks in $-\overline{u'w'}_{norm}$ were observed around $10h_d$ from the grass (Figures 6a and 6b), which are explored further in relation to Figure 7 (see later). The tree did not appear to induce large turbulent variations at the surface along most of the wake, but an increase in $-\overline{u'w'}_{norm}$ at 8–$10h_d$ suggests that the turbulence impacts of the crown may be felt at the surface much further downwind due to its elevation. The interaction between slower-moving wind in the lee of the crown and the faster-moving, unobstructed wind beneath the crown was likely responsible for strong increases in $-\overline{u'w'}_{norm}$ recorded up to $1h_d$, as well as the strongly negative $-\overline{u'w'}_{norm}$ values in the tree's wake at 1.50 m height.

Elements protruding into a boundary layer topographically force the wind to move around them to greater or lesser extents, thus impacting wind streamline angles. Figure 7 displays streamline angle variations in the vertical ($uw$) plane along the centreline of the element wake, together with changes in $\Phi$ and $-\overline{u'w'}_{norm}$. Upwind of the grass and shrub, the streamlines became more positive as the wind was forced upwards above the elements, and decreased as the wind flowed over the top of the plants. The effect was more pronounced above the grass clump than the shrub, and the streamline angle

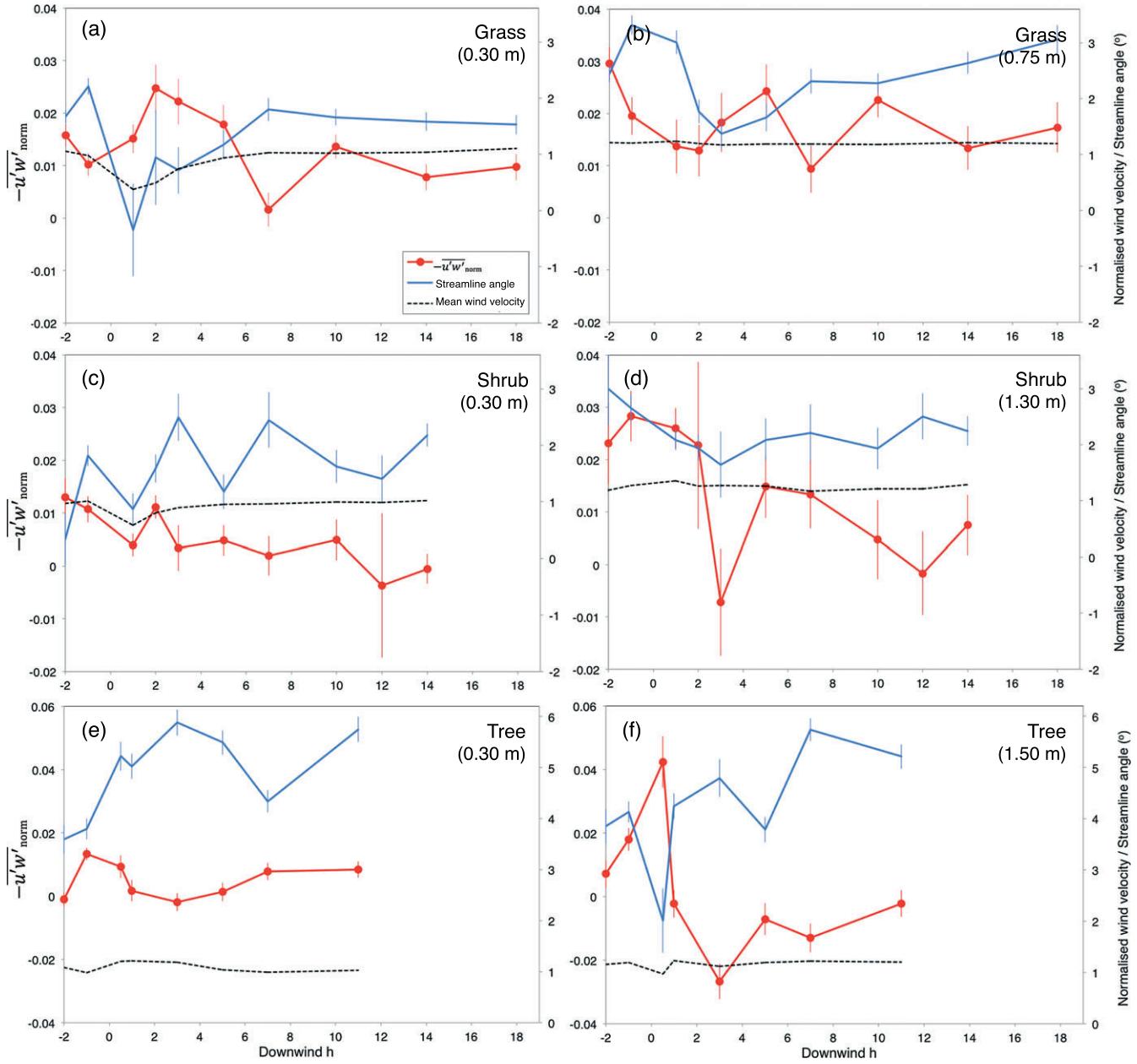


**Figure 7.** Variations in normalized Reynolds shear stress $\left(-\overline{u'w'}_{norm}\right)$, vertical streamline angle and normalized mean wind velocity ($\Phi$) at 0.30 m and height of elements (1.50 m for tree) along the centreline of: (a), (b) a grass; (c), (d) a shrub; (e), (f) a tree. Reynolds shear stress and wind velocity data were normalized to mean horizontal wind velocity measured upwind at 0.30 m height. Confidence intervals at the 95% level are shown as vertical bars. Downwind *h* for the tree is calculated using total tree height (trunk + crown). This figure is available in colour online at wileyonlinelibrary.com/journal/espl

became negative in the immediate lee of the grass. This is indicative of the formation of a small recirculation zone, which is expected to occur when low wind velocities in the immediate lee of a bluff element create a region of lower pressure that draws flow down and round towards its base (Hagen and Skidmore, 1971; Cornelis and Gabriels, 2005; Sutton and McKenna-Neuman, 2008; Lee *et al.*, 2014). There was no evidence for a recirculation zone in the lee of the shrub.

At 0.30 m height in the case of the grass and the shrub (Figures 7a and 7c), $-\overline{u'w'}_{norm}$ tended to increase where flow acceleration was strongest (i.e. as $\Phi$ was recovering most rapidly in the leeside wakes). Thereafter, $-\overline{u'w'}_{norm}$ tended to decrease as acceleration to $\Phi = 1$ was reduced. This pattern may be partly attributable to $u'$ and $w'$ peaks having a larger impact on shear stress calculations when average velocities are low. However, it is interesting to note that relatively large changes in turbulence occurred at the heights of both the grass and the shrub (Figures 7b and 7d), despite only minor corresponding changes in horizontal wind velocity. This suggests that peaks in turbulence at element height may result from different wind velocities at the surface and at element height driving a vertical exchange of small-scale turbulent eddies. In this way, surface turbulence in the lee of the elements is communicated upwards along the wake. Such a mechanism explains the simultaneous streamline angle increase at 0.30 m height and streamline angle decrease at the height of the elements in the flow recovery region (Figure 7). The smaller differences between flow velocity at the height of the shrub and at the surface compared to the grass, resulted in less shear at the top of the shrub and thus a weaker streamwise momentum transfer within the mixing zone (Judd *et al.*, 1996).

In the case of the tree (Figures 7e and 7f), the streamline angle tended to increase with increasing downwind distance. However, there was a strong decrease in streamline angle in

the lee of the trunk at 1.50 m height, which indicates an incursion of downward moving air as wind flow was deflected by the underside of the crown. Such a deflection process could be responsible for the large Reynolds shear stress values recorded beneath the crown, as well as the decreased wind velocities observed at 1.50 m height (Figure 2f). The streamline angle also decreased around 5–7$h_d$ at both heights, which was likely due to the air displaced over the top of the tree moving downwards and reconnecting with the surface flow.

Clearly, the relationships between individual Reynolds stress components, flow (de)acceleration and streamline angles around vegetation elements of differing porosities and configurations are complex. There is some evidence from Reynolds stress analysis that the bluff nature of the grass resulted in a more intense but less extensive impact on flow turbulence compared to the shrub. These differences may result from differential wind slowdown at the surface and at element height leading to varying intensities of vertical mixing and turbulent eddy exchange. However, it is difficult to separate the true covariance between $u'$ and $w'$ from the impact of flow velocity changes, as well as from topographically forced changes to the shape of the airflow. In order to segregate the stress budget between different structures in the flow around the elements, which in turn provides a way of assessing likely erosion and deposition zones, quadrant analysis (Lu and Willmarth, 1973; see Data analysis section) was conducted.

## Coherent flow structures

Previous aeolian studies have highlighted the importance of the coherency, or structured nature, of turbulence in the context of plant canopies (e.g. Finnigan, 1979; Shaw *et al.*, 1983; Yue *et al.*, 2007) and dunes (e.g. van Boxel *et al.*, 2004; Leenders *et al.*, 2005; Chapman *et al.*, 2012, 2013; Wiggs and Weaver, 2012). In the fluvial domain, a turbulent 'bursting process', whereby ejections (Q2) of low-velocity fluid from the wall region interact with sweeps (Q4) of high-velocity fluid towards the wall (Roy *et al.*, 1999), has been shown to be a key determinant of sediment transport (Best and Kostaschuk, 2002). The bursting process can be identified using the flow exuberance ($EX_{FL}$), defined as the ratio of total occurrence of outward (Q1) and inward (Q3) interactions to Q2 and Q4 events (Shaw *et al.*, 1983; Yue *et al.*, 2007; Chapman *et al.*, 2012). In effect, $EX_{FL}$ expresses the ratio of negative to positive contributions to Reynolds stress generation. Whilst exuberance describes the skewness of quadrant plot distributions, it does not account for the magnitudes of $u'$ and $w'$ that constitute the individual quadrant events. In our study, the absolute value of the $u'$ component for every occurrence of a given quadrant event ($|u'_{QX}|$) was averaged over the total measurement time at each location, and combined in the same ratio as flow exuberance. This provides a combined measure of the horizontal strength and occurrence of exuberance, $EX_{MAG}$:

$$EX_{MAG} = \frac{\overline{|u'_{Q1}|} + \overline{|u'_{Q3}|}}{\overline{|u'_{Q2}|} + \overline{|u'_{Q4}|}} \quad (2)$$

Figures 8a and 8b shows the variation in $EX_{MAG}$ along the centreline of the element wakes. $EX_{MAG}$ values for the grass remained relatively steady (0.6–0.7) at both heights, signifying an overall dominance of the power of ejections (Q2) and sweeps (Q4). At 0.30 m height in the case of the grass clump, $EX_{MAG}$ was at its minimum at 1$h_d$, supporting the notion that a small recirculation zone formed in the lee. A peak in $EX_{MAG}$ at 7$h_d$ suggests that Q1 and Q3 events became more important around the region of flow equilibration. $EX_{MAG}$ along the centreline of the shrub's wake was generally higher than for the grass at both heights, suggesting that the shrub acted to dampen the bursting process relative to the grass. In the case of the tree, $EX_{MAG}$ declined at both heights around the trunk before peaking significantly at 3$h_d$. The low exuberance observed around the trunk likely results from incursions of sweeps from within the tree crown, as previously reported in Large Eddy

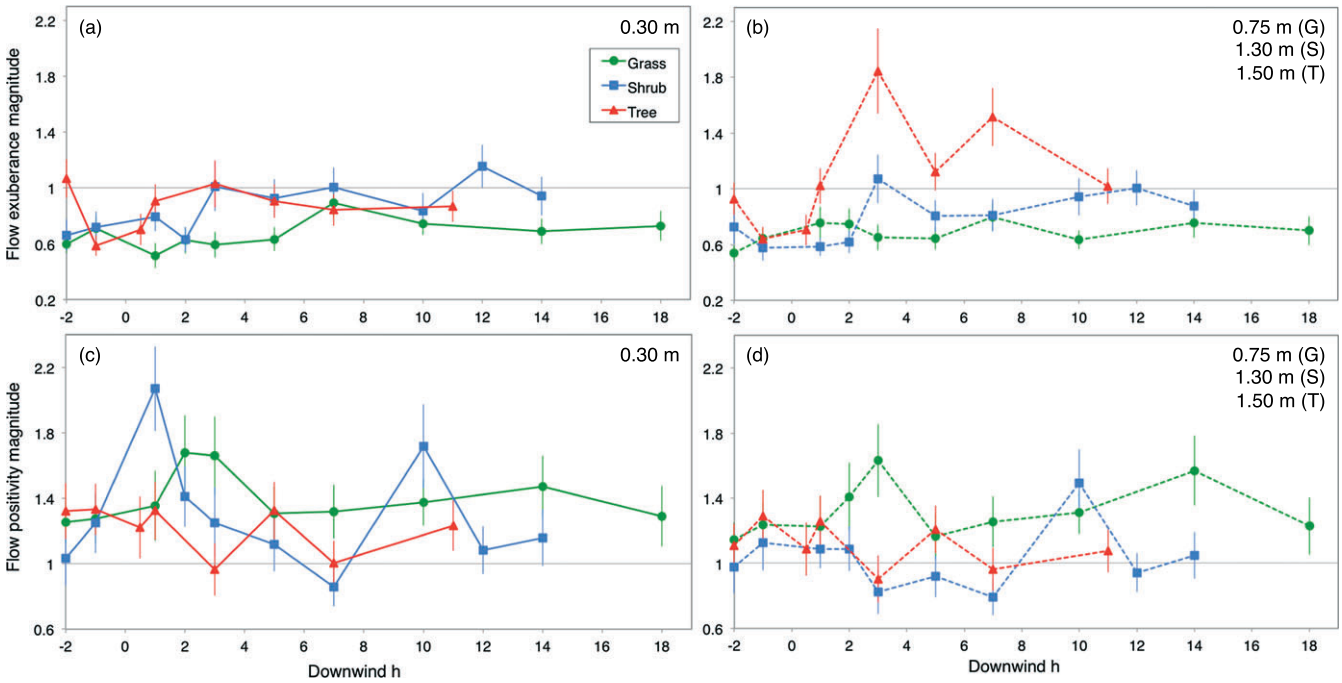


**Figure 8.** (a), (b) Horizontal magnitude of flow exuberance $\left(EX_{MAG} = \left(\left|\overline{u'_{Q1}}\right| + \left|\overline{u'_{Q3}}\right|\right)/\left(\left|\overline{u'_{Q2}}\right| + \left|\overline{u'_{Q4}}\right|\right)\right)$; and (c), (d) horizontal magnitude of flow positivity $\left(PO_{MAG} = \left(\left|\overline{u'_{Q1}}\right| + \left|\overline{u'_{Q4}}\right|\right)/\left(\left|\overline{u'_{Q2}}\right| + \left|\overline{u'_{3}}\right|\right)\right)$, along the centreline of each element wake at 0.30 m and element height (1.50 m for tree). Confidence intervals at the 95% level are shown as vertical bars. Downwind $h$ for the tree was calculated using total tree height (trunk + crown). Measurement heights are indicated in the top right corner of each panel. This figure is available in colour online at wileyonlinelibrary.com/journal/espl

Simulation (LES) studies (e.g. Shen and Leclerc, 1997; Su *et al.*, 1998; Yue *et al.*, 2007). The $EX_{MAG}$ peak at $3h_d$ implies the presence of an upwelling region, which likely corresponds to the formation of a relatively large vortical structure. This arises in the wake of trees due to momentum differences between the flow funnelled beneath the crown (the bottom gap) and the flow in a low-pressure region in the lee of the crown (Lee *et al.*, 2014). In this study, wind flow was not measured above 1.50 m and so the low-pressure region was not directly observed, but the existence of such a zone is likely given the low porosity (6%) of the tree crown. The occurrence of large $EX_{MAG}$ peaks in zones of strongly negative $-\overline{u'w'}$ (Figures 6e, 6f, 7e and 7f) confirms the presence of a counter-clockwise recirculation vortex in the wake of the tree (cf. Lee *et al.*, 2014). Across all three elements, the $-\overline{u'w'}$ parameter was strongly negatively correlated with $EX_{MAG}$ ($R^2 = 0.943$ at 0.30 m height and $R^2 = 0.842$ at 0.75 m height), because high Q1 and Q3 incidence is indicative of flow where $u'$ and $w'$ co-vary in the same relative direction.

Whilst the bursting process is well related to fluvial transport, there is increasing evidence (e.g. Sterk *et al.*, 1998; Schönfeldt and von Löwis, 2003; van Boxel *et al.*, 2004; Wiggs and Weaver, 2012; Chapman *et al.*, 2013) that aeolian transport is better associated with turbulent structures characterized by a positive streamwise fluctuating velocity ($u' > 0$, Q1 and Q4). This may be due to the greater disparity in density ratio between particles and wind compared to water (Wiggs and Weaver, 2012). Similarly to $EX_{MAG}$, the horizontal magnitude of the overall 'positivity' of the flow, $PO_{MAG}$, can be defined as the ratio of the mean absolute $u'$ for Q1 and Q4 events to Q2 and Q3 events:

$$PO_{MAG} = \frac{\overline{|u'_{Q1}|} + \overline{|u'_{Q4}|}}{\overline{|u'_{Q2}|} + \overline{|u'_{Q3}|}} \quad (3)$$

Flow positivity thus expresses the ratio of the strength of positive ($u' > 0$) to negative ($u' < 0$) contributions to streamwise velocity. Figures 8c and 8d shows the variation in $PO_{MAG}$ along the centreline of the three element wakes. Flow positivity tended to be higher in the wake of the grass compared to the shrub, although at $1h_d$ of the grass the small recirculation zone reduced the proportional incidence of Q1 and Q4 events. The peak in $PO_{MAG}$ at $2–3h_d$ of the grass (Figures 8c and 8d) is indicative of the strong positive component of the flow as it rapidly recovered behind the bluff element. In contrast, $PO_{MAG}$ increased significantly in the immediate lee of the shrub at 0.30 m height, suggesting that Q2 and Q3 events were dampened as the flow bled through the plant body. Moreover, $PO_{MAG}$ was significantly lower at the height of the shrub than at the surface. This difference in flow positivity across the two heights, which was absent in the case of the grass, resulted in momentum transfer being maintained much further downwind of the shrub than the grass. This explains the earlier peak in $\overline{u'^2}$ downwind of the grass (at $7h_d$; Figures 5a and 5b) compared to the shrub (at $10–12h_d$; Figures 5c and 5d). Along the centreline of the tree's wake, $PO_{MAG}$ values remained mainly above unity. The decrease in $PO_{MAG}$ at $3h_d$ from the tree likely corresponded to the reattachment of the counter-clockwise recirculation vortex in its wake, and the $PO_{MAG}$ decline at $7h_d$ probably resulted from airflow displaced over the tree crown moving downwards and reconnecting with the surface flow, thereby dissipating some of the wind's horizontal energy. Across all three elements, $-\overline{u'w'}$ was weakly correlated with $PO_{MAG}$ ($R^2 = 0.104$ at 0.30 m height and $R^2 = 0.162$ at 1.30 m height), due to contributions of Q1 and Q4 events offsetting each other in Reynolds stress calculations (Weaver and Wiggs, 2011; Chapman *et al.*, 2013)

This quadrant analysis shows that $EX_{MAG}$ and $PO_{MAG}$ patterns can be used to: (i) support the hypothesis that the bluff grass clump had a more intense but short-lived impact on flow turbulence than the shrub; (ii) confirm the existence of a recirculation zone in the lee of the grass; and (iii) identify the formation of a large vortical structure in the lee of the tree. The shrub generally dampened the bursting process (i.e. lower $EX_{MAG}$) and flow positivity ($PO_{MAG}$) to a greater extent than the grass, and induced lower $-\overline{u'w'}$, but it is not clear which of these turbulence parameters is appropriate for determining sediment transport potential. Whilst findings from dune-based studies imply that higher $PO_{MAG}$ or $-\overline{u'w'}$ might act to increase transport (Wiggs *et al.*, 1996b; Weaver and Wiggs, 2011; Chapman *et al.*, 2012, 2013; Wiggs and Weaver, 2012), evidence from Leenders *et al.* (2007) suggests that areas of high turbulence intensity in plant wakes are not necessarily associated with greater erosion, because they tend to be located within low-velocity zones where the energy of the flow is simply not large enough to entrain sediment. It is therefore difficult to identify zones of potential sediment transport around vegetation elements based simply on one or more turbulence parameters. In all likelihood, the combined impact of an element on both the mean and turbulent properties of the wind should be considered to adequately characterize the energy and variability of the flow at any point on a vegetated surface.

## Shelter effect

Perera (1981) proposed Gandemer's (1979) 'shelter parameter' ($\psi$) to express the overall sheltering effect of a windbreak, taking into account both the speedup/slowdown of wind and its streamwise turbulence. The parameter was later modified by Kim and Lee (2002) and Lee *et al.* (2014) to include the $w'$ component. However, vertical velocity variations in natural wind flow are roughly an order of magnitude smaller than the horizontal components (Sterk *et al.*, 1998), and the $w'$ component has been shown to be poorly correlated with aeolian sediment transport (Schönfeldt and von Löwis, 2003; Leenders *et al.*, 2005; Wiggs and Weaver, 2012), so Gandemer's (1979) original formulation for $\psi$ is used:

$$\psi = \frac{\left(|\overline{U}| + \sqrt{\overline{u'^2}}\right)}{\left(\overline{U}_{ref} + \sqrt{\overline{u'^2}_{ref}}\right)} \quad (4)$$

By combining the salient features of horizontal turbulent wind flow, the shelter parameter ($\psi$) provides a method of simultaneously accounting for the mean energy of the flow (i.e. $\bar{U}$) and the deviations away from it $\left(\overline{u'^2}\right)$. $\overline{u'^2}$ is used to characterize turbulence instead of the Reynolds shear stress ($-\overline{u'w'}$) because it better accounts for the streamwise variability that is thought to drive sediment transport in aeolian environments (e.g. Weaver and Wiggs, 2011). In Equation 4, lower $\psi$ values correspond to a greater sheltering effect, and vice versa.

The spatial variation of $\psi$ at 0.30 m height is shown in Figure 9. The grass induced a more intense sheltering zone in its lee than the shrub, which extended further downwind and laterally. These observations are statistically significant at the 95% level, given the distinct lack of overlap between the confidence bars of the grass and shrub curves in the immediate lee (Figure 9a). This implies that sediment transport for a given

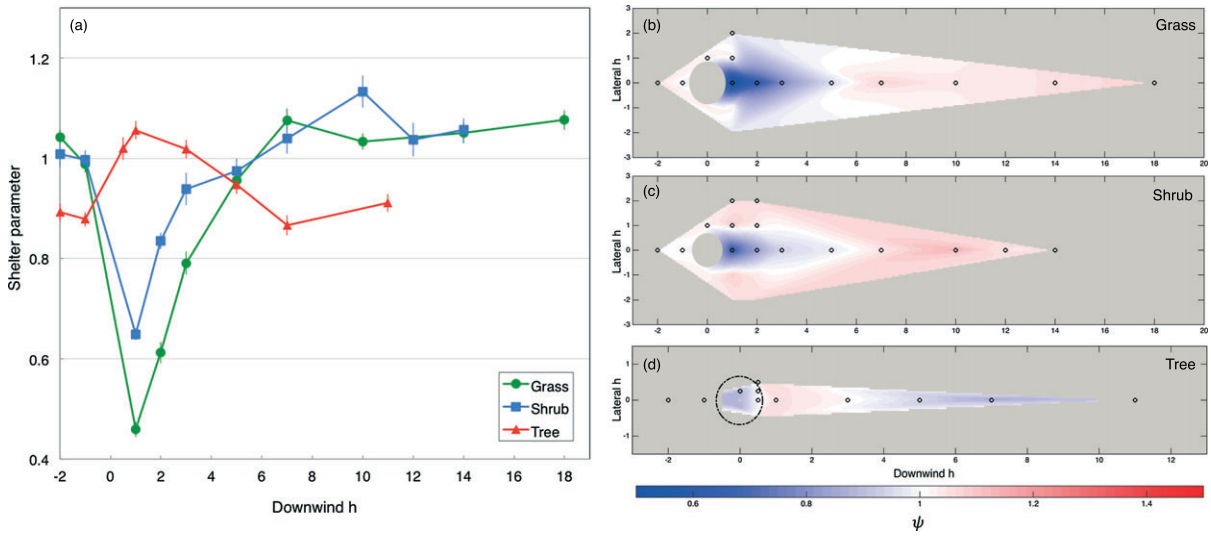


**Figure 9.** (a) Variations in the shelter parameter ($\psi$) along the centreline of the three element wakes at 0.30 m height. One-sigma error bars are shown; (b), (c), (d) Horizontal spatial patterns of $\psi$ around a grass, shrub and tree at 0.30 m height. Data were interpolated using a triangulation-based natural neighbour algorithm, with a grid spacing of 0.1 m. Locations of grass and shrub elements are shown by white ellipses. Tree crown is shown as a dotted ellipse. Black circles represent anemometer locations. Downwind $h$ for trees is calculated using total tree height (trunk + crown). Lateral turbulence data are mirrored across the centreline of each element wake. This figure is available in colour online at wileyonlinelibrary.com/journal/espl

approach wind velocity will tend to be lower in the wake of the grass compared to the wake of the shrub, even though full wind velocity recovery occurs at approximately the same distance downwind of both elements.

From $7h_d$ of both the grass and shrub, a zone of increased $\psi$ – and thus increased transport potential – was observed where the mixing layer intersected with the ground surface (cf. Judd *et al.*, 1996). This region was more extensive in the case of the shrub than the grass. The apparent 'overshoot' above $\psi$ = 1 may result from counter-rotating vortices induced by the elements creating a zone of elevated surface stress (Sutton and McKenna-Neuman, 2008; Burri *et al.*, 2011), which corresponds to the wind speedup observed at the sides of the shrub (Figure 2c). Walter *et al.* (2012) posited that the pliable nature of grassy plants results in grass clumps having a reduced sheltering effect at high wind speeds, due to a narrowing of the leeside wake and suppression of horseshoe vortices. The results presented here suggest that the bluff nature of the grass clump offsets this potential narrowing at the observed wind velocities, inducing a greater sheltering effect than a less pliable woody shrub. However, the shelter parameter had not recovered to unity by $18h_d$ in the grass case and $14h_d$ in the shrub case, suggesting flow was still being affected by the elements at these distances downwind.

In the case of the tree, there was a slight sheltering effect upwind of the trunk, but the general impact of the trunk and crown between $0.5h_d$ and $3h_d$ was to drastically decrease sheltering at the surface, primarily because of wind speedup linked to the bottom gap effect. This zone is therefore characterized by the highest sediment transport potential. Localized wind speedup around the trunk, which was not observed in the wind data but was inferred from a small topographical depression around the base of the trunk, also leads to increased localized erosion (Leenders *et al.*, 2007). From $3h_d$, where the frontal impact of the crown was increasingly felt at the surface, the tree sheltered the surface for at least eight tree heights.

While grasses and shrubs may trap sediment more readily than tall trees thanks to their low hanging branches and blades (Raupach *et al.*, 2001; Davidson-Arnott *et al.*, 2012), this study supports previous findings (Leenders *et al.*, 2007; Dupont *et al.*, 2014) that despite wind speedup resulting from a bottom gap, an elevated tree canopy extracts horizontal momentum from the air in such a way that a more extensive sheltering effect occurs downwind. Therefore, incorporating a parameter such as $\psi$ that emphasizes multiple salient features of horizontal turbulent flow, rather than relying entirely on wind velocity, may provide a better indicator of erosion potential around plants.

## Conclusions

Results from this study show that dryland grass, shrub and tree elements impact turbulent wind flow in differing ways. Wind velocity was reduced by 70% in the immediate lee of the grass clump and 40% in the lee of the shrub, but velocity recovered exponentially to equilibrium by ~$9h_d$ in both cases. This is comparable to the recovery lengths reported in previous studies for single elements. However, comparisons with existing models of wind recovery based on wind fence data (Hagen, 1996; Okin, 2008) suggest that wind flow downwind of 3D, partially bluff elements cannot be suitably parameterized using 2D analogues. Instead, a flow recovery curve of the form $ae^{-bx} + c$ produces a closer match with the field data in this study and with the empirically derived model of Leenders *et al.* (2011).

Despite the similar recovery distances of the grass and shrub, the bluff nature of the grass clump (53% porosity) induced more intense wind slowdown in its lee than the shrub (69% porosity). Bleed flow through the shrub was more significant than the grass, resulting in smaller differences between flow velocity at the surface and at the height of the shrub. This in turn led to lower shear stress and weaker vertical and streamwise exchange of small-scale turbulent eddies in the mixing zone of the shrub. The shrub therefore disrupted the airflow less intensely, but over a greater distance than the grass clump, as shown for the $\overline{u'^2}$ parameter. This supports previous findings (Skidmore and Hagen, 1970; Perera, 1981) that low-porosity elements induce turbulence in their lee but allow flow to recover to upstream conditions sooner than more porous elements. While the shrub generally dampened the bursting process [high ejection (Q2) and sweep (Q4) activity] and induced lower $-\overline{u'w'}$ than the grass, these turbulence parameters may not be wholly appropriate for determining sediment transport due to

the contradictions inherent to their calculation (Weaver and Wiggs, 2011; Chapman *et al.*, 2013). Instead, a parameter that emphasizes the salient features of horizontal turbulent flow such as the shelter parameter ($\psi$) may provide a better indicator of erosion potential around plants. Spatial analysis of $\psi$ in this study suggests that sediment transport potential is lower in the protective wake of the grass clump than in that of the shrub.

The tree produced a different wake structure to the grass clump and shrub, on account of its elevated canopy. The recovery of wind velocity downwind of the tree was best described using a logistic function ($a + ((b - c)/(1 - e^{x-d}))$ due to a 'bottom gap' effect (Ruck and Schmitt, 1986; Kim and Lee, 2002; Dupont *et al.*, 2014), whereby wind speeds up due to streamline compression in the gap between the ground and the underside of the tree crown. Differences in momentum arising between the flow funnelled through the bottom gap and the flow in the low-pressure leeward region are a probable explanation for the formation of a large recirculation vortex in the wake of the tree at ~$3h_d$. The bottom gap effect led to decreased sheltering beneath the crown and up to $3h_d$, but the surface became increasingly sheltered by the frontal impact of the crown over a further eight tree heights (~30 m) at least. Whilst trees are not capable of trapping saltating particles due to the height of their crowns, the extraction of momentum from the air by their elevated canopies could result in a far more extensive sheltering effect compared to grasses and shrubs.

This study provides important insights into the impacts of different vegetation types on turbulent wind flow. By characterizing the effects of key dryland plant types on local wind patterns, we build on existing parameterizations to provide a better constraint on the sheltering effects of vegetation. Since shifts in vegetation structure relating from environmental and anthropogenic stresses such as grazing, fire and climatic change have the potential to significantly impact sediment mobility in semi-arid regions, it is vital to improve our understanding of the aerodynamic behaviour of common dryland plant types. The new high-frequency data presented in this study can be integrated into robust, spatially explicit models of sediment transport and landscape change. This will contribute to answering key questions, at meaningfully large scales, about how semi-vegetated desert surfaces may respond to future environmental and anthropogenic stresses.

*Acknowledgements*—This research was funded by a UK Natural Environment Research Council Doctoral Training Grant (NE/L501530/1) and a St Catherine's College (Oxford) Scholarship to J.R.M. The authors thank P. and H. Möller and P. Swiegers for their kind permission to conduct fieldwork on their land, and are grateful to J. Nield and M. Baddock for fruitful methodological discussions. Two anonymous reviewers are thanked for their constructive comments.

## References

Al-Awadhi JM, Willetts BB. 1999. Sand transport and deposition within arrays of non-erodible cylindrical elements. *Earth Surface Processes and Landforms* **24**: 423–435.

Ash JE, Wasson RH. 1983. Vegetation and sand mobility in the Australian desert dunefield. *Zeitschrift für Geomorphologie (Supplement)* **45**: 7–25.

Baas ACW, Sherman DJ. 2005. Formation and behaviour of aeolian streamers. *Journal of Geophysical Research* **110**: F03011.

Baddock MC, Wiggs GFS, Livingstone I. 2011. A field study of mean and turbulent flow characteristics upwind, over and downwind of barchan dunes. *Earth Surface Processes and Landforms* **36**(11): 1435–1448. DOI. 10.1002/esp.2161

Bauer BO, Yi J, Namikas SL, Sherman DJ. 1998. Event detection and conditional averaging in unsteady aeolian systems. *Journal of Arid Environments* **39**: 345–375.

Best JL, Kostaschuk RA. 2002. An experimental study of turbulent flow over a low-angle dune. *Journal of Geophysical Research* **107**(C9): 3135. DOI. 10.1029/2000JC000294

van Boxel J, Sterk G, Arens S. 2004. Sonic anemometers in aeolian sediment transport research. *Geomorphology* **59**(1–4): 131–147.

Bradley EF, Mulhearn PJ. 1983. Development of velocity and shear-stress distributions in the wake of a porous shelter fence. *Journal of Wind Engineering and Industrial Aerodynamics* **15**(1–3): 145–156.

Burri K, Gromke C, Lehning M, Graf F. 2011. Aeolian sediment transport over vegetation canopies: a wind tunnel study with live plants. *Aeolian Research* **3**: 205–213.

Butterfield GR. 1991. Grain transport rates in steady and unsteady turbulent airflows. *Acta Mechanica (Supplement)* **1**: 97–122.

Butterfield GR. 1993. Sand transport response to fluctuating wind velocity. In Turbulence: Perspectives on Sediment Transport, Clifford NJ, French JR, Hardisty J (eds). John Wiley & Sons: Chichester; 305–334.

Chapman CA, Walker IJ, Hesp PA, Bauer BO, Davidson-Arnott RGD. 2012. Turbulent Reynolds stress and quadrant event activity in wind flow over a coastal foredune. *Geomorphology* **151–152**: 1–12.

Chapman C, Walker IJ, Hesp PA, Bauer BO, Davidson-Arnott RGD, Ollerhead J. 2013. Reynolds stress and sand transport over a foredune. *Earth Surface Processes and Landforms* **38**(14): 1735–1747.

Clifford NJ, French JR. 1993. Monitoring and modelling turbulent flows: historical and contemporary perspectives. In Turbulence: Perspectives on Flow and Sediment Transport, Clifford NJ, French JR, Hardisty J (eds). John Wiley & Sons: New York; 1–34.

Cornelis WM, Gabriels D. 2005. Optimal windbreak design for wind-erosion control. *Journal of Arid Environments* **61**(2): 315–332.

Crawley DM, Nickling WG. 2003. Drag partition for regularly-arrayed rough surfaces. *Boundary Layer Meteorology* **107**: 445–468.

Davidson-Arnott RGD, Bauer BO, Walker IJ, Hesp PA, Ollerhead J, Chapman C. 2012. High-frequency sediment transport responses on a vegetated foredune. *Earth Surface Processes and Landforms* **37** (11): 1227–1241.

Dupont S, Bergametti G, Simoëns S. 2014. Modeling aeolian erosion in presence of vegetation. *Journal of Geophysical Research, Earth Surface* **119**(2): 168–187. DOI. 10.1002/2013JF002875

Finnigan JJ. 1979. Turbulence in waving wheat: 1. Mean statistics and honami. *Boundary Layer Meteorology* **16**: 181–211.

Frank A, Kocurek G. 1996. Airflow up the stoss slope of sand dunes: limitations of current understanding. *Geomorphology* **17**: 47–54.

Gandemer J. 1979. Wind shelters. *Journal of Wind Engineering and Industrial Aerodynamics* **4**: 371–389.

van Gardingen P, Grace J. 1991. Plants and wind. *Advances in Botanical Research* **18**: 189–253.

Gillette DA, Stockton PA. 1989. The effects of non-erodible particles on wind erosion of erodible surfaces. *Journal of Geophysical Research* **94**(D10): 12885–12893.

Gillette DA, Herrick JE, Herbert GA. 2006. Wind characteristics of Mesquite Streets in the northern Chihuahuan Desert, New Mexico, USA. *Environmental Fluid Mechanics* **6**(3): 241–275.

Gillies JA, Lancaster N, Nickling WG, Crawley D. 2000. Field determination of drag forces and shear stress partitioning effects for a desert shrub (*Sarcobatus vermiculatus*, Greasewood). *Journal of Geophysical Research: Atmosphere* **105**(D20): 24871–24880.

Gillies JA, Nickling WG, King J. 2002. Drag coefficient and plant form-response to wind velocity in three plant species: Burning bush (Euonymus alatus), Colorado blue spruce (*Picea pungens* glauca.), and fountain grass (*Pennisetum setaceum*). *Journal of Geophysical Research* **107**(D24): 4760.

Gillies JA, Nield JM, Nickling WG. 2014. Wind velocity and sediment transport recovery in the lee of a vegetated and denuded nebkha within a nebkha dune field. *Aeolian Research* **12**: 135–141.

Grant PF, Nickling WG. 1998. Direct field measurement of wind drag on vegetation for application to windbreak design and modeling. *Land Degradation and Development* **9**: 57–66.

Gross G. 1987. A numerical study of the air flow within and around a single tree. *Boundary-Layer Meteorology* **40**: 311–327.

Hagen LJ. 1996. WEPS: Wind Erosion Prediction System, Technical Documentation. Wind Erosion Research Unit: Manhattan, NY.

Hagen LJ, Skidmore EL. 1971. Turbulent velocity fluctuations and vertical flow as affected by windbreak porosity. *Transactions of the American Society of Agricultural Engineers* **14**: 634–637.

Judd MJ, Raupach MR, Finnigan JJ. 1996. A wind tunnel study of turbulent flow around single and multiple windbreaks. Part I: velocity fields. *Boundary Layer Meteorology* **80**: 127–165.

Kenney WA. 1987. A method for estimating windbreak porosity using digitized photographic silhouettes. *Agricultural and Forest Meteorology* **39**: 91–94.

Kim HB, Lee S-J. 2002. The structure of turbulent shear flow around a two-dimensional porous fence having a bottom gap. *Journal of Fluids and Structures* **16**(3): 317–329.

King J, Nickling WG, Gillies JA. 2005. Representation of vegetation and other non-erodible elements in aeolian shear stress partitioning models for predicting transport threshold. *Journal of Geophysical Research* **110**: F04015.

Lapointe MF. 1992. Burst-like sediment suspension events in a sand bed river. *Earth Surface Processes and Landforms* **17**: 253–270.

Lee SJ, Park KC, Park CW. 2002. Wind tunnel observations about the shelter effect of porous fences on the sand particle movements. *Atmospheric Environment* **36**: 1453–1463.

Lee J-P, Lee E-J, Lee S-J. 2014. Shelter effect of a fir tree with different porosities. *Journal of Mechanical Science and Technology* **28**(2): 565–572. DOI. 10.1007/s12206-013-1123-6

Leenders JK, van Boxel JH, Sterk G. 2005. Wind forces and related saltation transport. *Geomorphology* **71**: 357–372.

Leenders JK, van Boxel JH, Sterk G. 2007. The effect of single vegetation elements on wind velocity and sediment transport in the Sahelian zone of Burkina Faso. *Earth Surface Processes and Landforms* **32**(10): 1454–1474.

Leenders JK, Sterk G, van Boxel JH. 2011. Modelling wind-blown sediment transport around single vegetation elements. *Earth Surface Processes and Landforms* **36**(9): 1218–1229. DOI. 10.1002/esp.2147

Li J, Okin GS, Alvarez L, Epstein H. 2008. Effects of wind erosion on the spatial heterogeneity of soil nutrients in two desert grassland communities. *Biogeochemistry* **88**: 73–88.

Li J, Okin GS, Herrick JE, Belnap J, Miller ME, Vest K, Draut AE. 2013. Evaluation of a new model of aeolian transport in the presence of vegetation. *Journal of Geophysical Research, Earth Surface* **118**(1): 288–306.

Lu SS, Willmarth WW. 1973. Measurements of the structure of Reynolds' stress in a turbulent boundary layer. *Journal of Fluid Mechanics* **60**: 481–511.

MacKinnon DJ, Clow GD, Tigges RK, Reynolds RL, Chavez JPS. 2004. Comparison of aerodynamically and model-derived roughness lengths (Zo) over diverse surfaces, central Mojave Desert, California, USA. *Geomorphology* **63**: 103–113.

Minvielle F, Marticorena B, Gillette DA, Lawson RE, Thompson R, Bergametti G. 2003. Relationship between the aerodynamic roughness length and the roughness density in cases of low roughness density. *Environmental Fluid Mechanics* **3**: 249–267.

Musick HB, Trujillo SM, Truman CR. 1996. Wind-tunnel modelling of the influence of vegetation structure on saltation threshold. *Earth Surface Processes and Landforms* **21**(7): 589–605.

Namikas SL. 2003. Field measurement and numerical modelling of aeolian mass flux distributions on a sandy beach. *Sedimentology* **50**(2): 303–326.

Okin GS. 2008. A new model of wind erosion in the presence of vegetation. *Journal of Geophysical Research* **113**(F2): F02S10.

Okin GS, Gillette DA, Herrick JE. 2006. Multi-scale controls on and consequences of aeolian processes in landscape change in arid and semi-arid environments. *Journal of Arid Environments* **65**(2): 253–275.

Perera MDAES. 1981. Shelter behind two-dimensional solid and porous fences. *Journal of Wind Engineering and Industrial Aerodynamic* **8**: 93–104.

Raupach MR. 1992. Drag and drag partition on rough surfaces. *Boundary-Layer Meteorology* **60**(4): 375–395.

Raupach MR, Woods N, Dorr G, Leys JF, Cleugh HA. 2001. The entrapment of particles by windbreaks. *Atmospheric Environment* **35**: 3373–3383.

Ravi S, D'Odorico P, Breshears DD, Field JP, Goudie AS *et al*. 2011. Aeolian processes and the biosphere. *Review of Geophysics* **RG3001**: 1–45.

van Rooyen N, Bezuidenhout H, de Kock E. 2001. Flowering Plants of the Kalahari Dunes. Ekotrust: Pretoria.

Roy AG, Biron PM, Buffin-Bélanger T, Levasseur M. 1999. Combined visual and quantitative techniques in the study of natural turbulent flows. *Water Resource Research* **35**: 871–877. DOI. 10.1029/1998WR900079

Ruck VB, Schmitt F. 1986. Das Strömungsfeld der Einzelbaumuströmung. Abschätzung von Depositionswahrscheinlichkeiten für Feinsttröpfchen. *Forstwissenschaftliches Centralblatt* **105**: 178–196.

Sankey JB, Ravi S, Wallace CSA, Webb RH, Huxman TE. 2012. Quantifying soil surface change in degraded drylands: shrub encroachment and effects of fire and vegetation removal in a desert grassland. *Journal of Geophysical Research, Biogeosciences* **117**(G2): 1–11.

Schönfeldt HJ, von Löwis S. 2003. Turbulence-driven saltation in the atmospheric surface layer. *Meteorologische Zeitschrift* **12**(5): 257–268.

Shaw RH, Tavangar T, Ward DP. 1983. Structure of the Reynolds stress in the canopy layer. *Journal of Climate and Applied Meteorology* **22**: 1922–1931.

Shen S, Leclerc MY. 1997. Modelling the turbulence structure in the canopy layer. *Agricultural Forest Meteorology* **87**: 3–25.

Smith CR. 1996. Coherent flow structures in smooth-wall turbulent boundary layers: facts, mechanisms and speculation. In Coherent Flow Structures in Open Channels, Ashworth PJ, Bennett SJ, Best JL, McLelland SJ (eds). John Wiley & Sons: New York; 1–39.

Sterk G. 2000. Flattened residue effects on wind speed and sediment transport. *Soil Science Society of America Journal* **64**: 852–858.

Sterk G, Jacobs AFG, van Boxel JH. 1998. The effect of turbulent flow structures on saltation sand transport in the atmospheric boundary layer. *Earth Surface Processes and Landforms* **23**(10): 877–887.

Stewart J, Parsons AJ, Wainwright J, Okin GS, Bestelmeyer B, Fredrickson EL, Schlesinger WH. 2014. Modelling emergent patterns of dynamic desert ecosystems. *Ecological Monographs* **84**(3): 373–410.

Su H-B, Shaw RH, Paw KT, Moeng CH, Sullivan PP. 1998. Turbulent statistics of neutrally stratified flow within and above a sparse forest from large-eddy simulation and field observations. *Boundary Layer Meteorology* **88**: 363–397.

Suter-Burri K, Gromke C, Leonard KC, Graf F. 2013. Spatial patterns of aeolian sediment deposition in vegetation canopies: observations from wind tunnel experiments using colored sand. *Aeolian Research* **8**: 65–73. DOI. 10.1016/j.aeolia.2012.11.002

Sutton SLF, McKenna-Neuman C. 2008. Sediment entrainment to the lee of roughness elements: effects of vortical structures. *Journal of Geophysical Research* **113**: F02S09.

Taylor PA. 1988. Turbulent wakes in the boundary layer. In Flow and Transport in the Natural Environment: Advances and Applications, Steffen WL, Denmead OT (eds). Springer-Verlag: Berlin; 270–292.

Tegen I, Harrison SP, Kohfeld K, Prentice C, Coe M, Heimann M. 2002. Impact of vegetation and preferential source areas on global dust aerosol: results from a model study. *Journal of Geophysical Research* **107**(D21): 4576.

Thomas DSG, Leason HC. 2005. Dunefield activity response to climate variability in the southwest Kalahari. *Geomorphology* **64**(1–2): 117–132. DOI. 10.1016/j.geomorph.2004.06.004

Thomas DSG, Knight M, Wiggs GFS. 2005. Remobilization of southern African desert dune systems by twenty-first century global warming. *Nature* **435**(7046): 1218–1221.

Vigiak O, Sterk G, Warren A, Hagen LJ. 2003. Spatial modeling of wind speed around windbreaks. *Catena* **52**(3–4): 273–288. DOI. 10.1016/S0341-8162(03)00018-3

Walker IJ. 2005. Physical and logistical considerations of using ultrasonic anemometry in aeolian sediment transport research. *Geomorphology* **68**: 57–76.

Walter B, Gromke C, Leonard KC, Manes C, Lehning M. 2012. Spatio-temporal surface shear-stress variability in live plant canopies and cube arrays. *Boundary-Layer Meteorology* **143**(2): 337–356.

Wang H, Takle ES. 1996. Momentum budget and shelter mechanism of boundary-layer flow near a shelterbelt. *Boundary-Layer Meteorology* **82**: 417–435.

Wang X, Yang Y, Dong Z, Zhang C. 2009. Responses of dune activity and desertification in China to global warming in the twenty-first century. *Global and Planetary Change* **67**: 167–185.

Wasson RJ, Nanninga PM. 1986. Estimating wind transport of sand on vegetated surfaces. *Earth Surface Processes and Landforms* **11**: 505–514.

Weaver CM. 2008. Turbulent Flow and Sand Dune Dynamics: Identifying Controls on Aeolian Sediment Transport, Unpublished PhD Thesis. University of Oxford.

Weaver CM, Wiggs GFS. 2011. Field measurements of mean and turbulent airflow over a barchan sand dune. *Geomorphology* **128**(1–2): 32–41.

Wiggs GFS, Weaver CM. 2012. Turbulent flow structures and aeolian sediment transport over a barchan sand dune. *Geophysical Research Letters* **39**(5): 1–7.

Wiggs GFS, Livingstone I, Thomas DSG, Bullard JE. 1994. Effect of vegetation removal on airflow patterns and dune dynamics in the southwest Kalahari Desert. *Land Degradation and Rehabilitation* **5**: 13–24.

Wiggs GFS, Thomas DSG, Bullard JE, Livingstone I. 1995. Dune mobility and vegetation cover in the southwest Kalahari Desert. *Earth Surface Processes and Landforms* **20**(6): 515–529.

Wiggs GFS, Livingstone I, Thomas DSG, Bullard JE. 1996a. Airflow and roughness characteristics over partially vegetated linear dunes in the southwest Kalahari Desert. *Earth Surface Processes and Landforms* **21**: 19–34. DOI. 10.1002/(SICI)1096-9837(199601)21:1 < 19::AID-ESP508 > 3.0.CO;2-P

Wiggs GFS, Livingstone I, Warren A. 1996b. The role of streamline curvature in sand dune dynamics: Evidence from field and wind tunnel measurements. *Geomorphology* **17**(1–3): 29–46. DOI. 10.1016/0169-555X(95)00093-K

Wolfe SA, Nickling WG. 1993. The protective role of sparse vegetation in wind erosion. *Progress in Physical Geography* **17**: 50–68.

Wu X, Zou X, Zhou N, Zhang C, Shi S. 2015. Deceleration efficiencies of shrub windbreaks in a wind tunnel. *Aeolian Research* **16**: 11–23. DOI. 10.1016/j.aeolia.2014.10.004

Youssef F, Visser SM, Karssenberg D, Erpul G, Cornelis WM, Gabriels D, Poortinga A. 2012. The effect of vegetation patterns on wind-blown mass transport at the regional scale: a wind tunnel experiment. *Geomorphology* **159–160**: 178–188. DOI. 10.1016/j.geomorph.2012.03.023

Yue W, Meneveau C, Parlange MB, Zhu W, van Hout R, Katz J. 2007. A comparative quadrant analysis of turbulence in a plant canopy. *Water Resources Research* **43**(5): 2–15. DOI. 10.1029/2006WR005583